

# Simulating the effects of inelastic scattering on upwelling radiance in coastal and inland waters: implications for hyperspectral remote sensing

J. Vigneshwaran, P. Shanmugam\* and E. A. Gokul

Ocean Optics and Imaging Laboratory, Department of Ocean Engineering, Indian Institute of Technology Madras, Chennai 600 036, India

Successful interpretation of spectral images from hyperspectral sensors is particularly important to achieve some far-reaching goals, including the detection and assessment of harmful algal blooms, water quality characteristics, trophic status of water bodies and marine/freshwater primary production. The present work is motivated by the desire to study the effect of inelastic scattering (chlorophyll and gelbstoff fluorescence and water Raman scattering) on upwelling radiance through a direct method. The contribution of inelastic scattering to the emergent (upwelling) radiance from the water column is of significant importance and has relevance for the hyperspectral remote sensing of water colour. The method introduced to simulate inelastic scattering is a straightforward approach and differs from previous work in the way of derivation. The model allows for simulation of upwelling radiance for clear, turbid and productive (phytoplankton-dominated) waters. The results of this model are assessed by comparison with depth-

dependant upwelling radiance data and results from the Hydrolight numerical model for these three water types. The comparisons show good agreement between measured and simulated values from the present model. The errors of this model are significantly small (when compared with those of the Hydrolight model) in the red wavelength region, where the chlorophyll fluorescence emission tends to peak around 685–720 nm when the concentration of chlorophyll is high in productive eutrophic waters. The magnitude and peak position at these wavelengths as produced by the present model could be used as precise indicators and predictors for the phytoplankton concentration in marine and inland water bodies. Thus, this work will have important implications in refining hyperspectral bio-optical algorithms for fluorescence and water Raman scattering as well as for the high concentrations and variabilities of water constituents in coastal and inland regions, and in evaluating remote sensing reflectance measurements of these water bodies.

**Keywords:** Inelastic scattering, phytoplankton CDOM fluorescence, Raman scattering, turbid and productive waters.

## Introduction

THE upwelling radiance  $L_u(\lambda)$  from the upward vertical (zenith angle equal to steradians), measured using underwater profiling radiometers, or the radiance leaving the sea  $L_w(\lambda)$  at nadir and quantified 'just above' the surface by taking into account refraction and reflection at the interface, measured using above-water radiometers<sup>1</sup> or derived from ocean-colour sensor measurements after the atmospheric correction (thus its angle is defined by the viewing angle and position of the satellite sensor)<sup>2,3</sup>, is an important parameter in ocean colour remote sensing<sup>1,4</sup>. This emergent radiance from the ocean is affected by chlorophyll and gelbstoff fluorescence as well as water

Raman scattering, which are considered important inelastic processes and have become of great interest in hydrologic optics since they can appreciably affect the spectral distribution of upwelling radiance and hence influence the signal available for remote sensing in the visible region<sup>5-7</sup>. Recent simulation results suggest that water Raman scattering can contribute significantly to the upwelling radiance field across all visible wavelengths to a variable degree<sup>8</sup>, thereby preventing optical closure efforts using hyperspectral radiometric field measurements<sup>9</sup> and introducing uncertainty to models relating the radiance field to the inherent optical properties (IOPs) of the ocean. This implies that water Raman scattering effect cannot be simply ignored in ocean colour modelling. Thus, efforts have been made to include this part of the inelastic scattering in semi-empirical algorithms to invert *in situ* or satellite ocean colour radiance or reflectance data<sup>10,11</sup>. On the contrary, a significant part of the inelastic scattering process is dominated by coloured dissolved organic matter (CDOM or 'gelbstoff') through fluorescence in the blue to red domain, which is generally

\*For correspondence. (e-mail: pshanmugam@iitm.ac.in)

believed due solely to particulate organic materials (chlorophyll pigment contained algal particles). CDOM contribution to elastic scattering is most often neglected, but there is observational evidence based on laboratory culture experiments that fluorescent dissolved organic matter (FDOM) produced by bloom-forming coastal and inland water phytoplankton can significantly contribute to inelastic scattering in the blue and red wavelengths<sup>12</sup>, while there is lack of knowledge of its contribution to the upwelling radiance for more turbid and eutrophic coastal/inland waters.

Chlorophyll fluorescence is another important inelastic process, and has been known to contribute to the upwelling radiance in the wavelength range from 685 to 730 nm by virtue of the chlorophyll pigment contained in phytoplankton. As a result, its contribution to the upwelling radiance, especially in productive waters (eutrophic water bodies) is evident by its distinct spectral signature with a peak around this wavelength region<sup>13,14</sup> attributed to enhanced chlorophyll fluorescence and a local minimum in total absorption. A simultaneous quantitative analysis of these two possible causes has not been adequately conducted for eutrophic–hypertrophic marine and inland waters. Though the effect of chlorophyll fluorescence on the water-leaving radiance has already been investigated by several authors<sup>11,15–17</sup>, there is still a lack of knowledge for turbid and eutrophic waters that are characterized by the complex mix of both a higher content of chlorophyll, suspended sediments and coloured dissolved organics as well as covarying, to completely independent, mixtures of these variable concentrations<sup>18</sup>.

All these water constituents eventually cause different optical processes such as absorption, scattering, and fluorescence and subsequently modify the underwater light fields in a wavelength, depth and angular-dependent way<sup>5</sup>. The link between these optical processes and radiance field can be mathematically described by the radiative transfer equation (RTE). In this work, the RTE for a fluorescent medium (dominated by phytoplankton) is solved in order to determine upwelling radiance from different depths, which is the important radiometric quantity required for many ocean colour applications. Here, the way of solving the RTE and deriving a model to deal with inelastic scattering is a straightforward process and differs from the existing models. Additionally, CDOM fluorescence and water Raman scattering are also included to investigate their contribution to the upwelling radiance. All these three parts lead to inelastic scattering of incident photons in natural water bodies. The simulated upwelling radiances for different waters are assessed by comparison with measured data and results from the Hydrolight numerical model. The sensitivity of upwelling radiance to individual and concerted impacts of the above trans-spectral processes, and to variations in the concentration of the major optically active substances is further investigated and discussed.

## Data and methods

### *In situ data*

The underwater vertical profiles of IOPs (inherent optical properties) and AOPs (apparent optical properties) were collected in turbid coastal waters off Point Calimere and clear waters off Chennai during two cruises (August 2013 and January 2014). Similar *in situ* data were obtained from turbid productive (algal-bloom dominated) waters around Chennai during December 2013 and March 2014. It is a backwater system connected to the Bay of Bengal and located about 30 km south of Chennai. Further information regarding these datasets is given in Table 1.

### *Measurement of IOPs*

The depth profiles of the particulate absorption  $a_p(\lambda)$  and attenuation  $c_p(\lambda)$  coefficients in the visible wavelengths (350–750 nm) were obtained with an AC-S instrument (WETLAB Inc) and corrected for the temperature, salinity and scattering effects that introduced systematic errors associated with incomplete collection and rejection of scattered photons within the measurement systems. The pure water absorption and scattering coefficients were taken from Pope and Fry<sup>19</sup>, and Smith and Baker<sup>20</sup> and added to the  $a_p(\lambda)$  and  $c_p(\lambda)$  coefficients in order to obtain the total absorption  $a(\lambda)$  and attenuation  $c(\lambda)$  coefficients. The backscattering measurements were made at nine wavelengths (412, 440, 488, 510, 532, 595, 650, 676 and 715 nm) using an ECO-BB9 profiling instrument (WETLAB, Inc). The chlorophyll and turbidity profiles were obtained using the FLNTU sensors and the conductivity–temperature–depth profiles were measured with a SBE-CTD sensor to support the above data processing and analyses.

### *Measurement of AOPs*

The RAMSES (Trios) ARC and ACC hyperspectral radiometers were used to measure upwelling radiance and downwelling irradiance in the visible and near-infrared region (350–950 nm). These sensors were mounted on a frame and deployed in water through a winch system and the acquired data were transmitted to a PC on the deck. Each observation was viewed and processed using the software MSDA\_XE. Since the sensors were immersed in water, the immersion factors (wavelength-dependent correction factors) were also considered.

### *Radiative transfer equation*

The transformation of the underwater light field is due to numerous processes and can be described by the RTE,

**Table 1.** Details of sampling stations

Station	Date	Time	Latitude	Longitude	Depth (m)
St-1	31 August 2013	10.30	13°14.525'N	80°35.068'E	20
St-2	28 January 2014	10.30	18°19.420'N	79°57.872'E	5
St-3	16 December 2013	14.15	12°82.208'N	80°24.05'E	1–2
St-4	19 March 2014	13.00	12°82.208'N	80°24.05'E	1–2
St-5	19 March 2014	13.15	12°82.208'N	80°24.05'E	1–2

which gives the mathematical representation of physical processes (phenomenon) of energy transfer in the form of electromagnetic radiation (EMR). It is the basis for various direct models, which attempt to simulate underwater radiance field from the measured IOPs. To achieve this there exist several radiative transfer methods, including the discrete-ordinate (DISORT) method, invariant embedding method, adding and doubling method, matrix operator method, spherical harmonics method, multi-component method, spherical harmonics discrete ordinate method, FN method, successive order of scattering (SOS) method, Monte Carlo method and Hydrolight numerical model. Among these, the Hydrolight model is widely used by the ocean optics community, though it poses some issues for turbid coastal waters<sup>4</sup>. The basic form of the RTE is expressed as

$$\mu \frac{dL(z, \xi, \lambda)}{dz} = -c(z, \lambda)L(z, \xi, \lambda) + \int_{\Xi} L(z, \xi', \lambda) \beta(z, \xi' \rightarrow \xi, \lambda) d\Omega(\xi') + S(z, \xi, \lambda), \quad (1)$$

where  $L$  is the radiance,  $\xi$  the direction,  $z$  the geometric depth,  $\lambda$  the wavelength,  $\Omega$  the solid angle,  $\beta$  the volume scattering function,  $S$  the source function, and  $c$  is the total attenuation coefficient. The source term  $S(z, \xi, \lambda)$  can describe either an internal light source such as bioluminescence, or inelastic scattering from other wavelengths (i.e. water Raman scattering and fluorescence due to chlorophyll and gelbstoff). Inputting IOPs along the depth, the RTE can be solved numerically for the radiance distribution.

#### *Hydrolight numerical model*

The Hydrolight model is a numerical model based on the invariant imbedding solution technique that computes spectral radiance distribution. Once the spectral radiance is known, all other optical quantities such as irradiance and reflectance can be computed from their definitions. The invariant imbedding is restricted to problems with only one spatial dimension and to simple boundary conditions (e.g. flat surface and bottom). In general, the Hydrolight code includes the effects of inelastic scatter-

ing due to chlorophyll fluorescence, CDOM fluorescence as well as water Raman scattering. Given the IOPs throughout a medium, the nature of the wind-blown sea surface and the bottom of the water column, and the sun and sky radiance incident on the sea surface as input to this model, one can obtain the spectral radiance distribution as a function of depth, direction and wavelength within and leaving the medium<sup>21</sup>.

#### *Model description*

In this study, the RTE is solved analytically to compute the upwelling radiance ( $L_u(\lambda)$ ). Since chlorophyll and gelbstoff fluorescence as well as water Raman scattering are important sources of inelastic scattering, these three terms are derived and included in the RTE (eq. (1)). The derivation is based on solving the RTE, which is straightforward and differs from other studies. The resultant first-order differential equation is solved based on the assumption that the IOPs for a particular depth interval ( $\Delta z$ ) are constant and the  $\Delta z$  value varies according to the nature of water as shown in Figure 1. The  $\Delta z$  values are inversely proportional to the turbidity of water. If the turbidity is more,  $\Delta z$  values are less and vice versa. The solutions to different inelastic scattering source functions are discussed below.

#### *Inelastic scattering*

The inelastic scattering is often referred to as trans-spectral<sup>22</sup>, since stimulation at wavelength  $\lambda'$  leads to emissions at  $\lambda$ , where, in general,  $\lambda > \lambda'$ . Note that water Raman scattering is a slightly different process from other forms of absorption-reemission interactions (such as fluorescence from CDOM and chlorophyll), being associated with a nearly fixed spectral shift between excitation and emission frequencies<sup>23</sup>. The process of inelastic scattering on the upwelling radiance can be expressed as the additive consequences of each energy transfer process occurring within the water column, namely

$$L_u(\lambda, z) = L_{u,R}(\lambda, z) + L_{u,F,chl}(\lambda, z) + L_{u,F,CDOM}(\lambda, z), \quad (2)$$

where  $L_{u,R}$  is the contribution from water Raman scattering,  $L_{u,F,chl}$  the contribution from fluorescence from

chlorophyll and  $L_{u,F,CDOM}$  is the contribution from fluorescence from coloured dissolved organic matter (coloured dissolved organics or gelbstoff).

The inelastic source function is expressed as

$$S = \int_0^\lambda \int_{4\pi} \beta(z, \xi' \rightarrow \xi, \lambda' \rightarrow \lambda) L(z, \xi', \lambda') d\Omega(\xi') d\lambda'. \quad (3)$$

*Water Raman scattering*

Mobley<sup>21</sup> mathematically described the contribution of water Raman scattering to the phase function in natural water bodies. Here the water molecules exchange energy with incoming photons and re-emit the energy approximately at the same wavelength, but with small shifts approximately  $3400 \text{ cm}^{-1}$  near the longer or shorter wavelengths. The source function for water Raman scattering by which the photons are absorbed at the incident wavelength  $\lambda'$  and re-emitted at different wavelengths, is as given below

$$S_R = \int_0^\lambda \int_{4\pi} \beta_R(z, \xi' \rightarrow \xi, \lambda' \rightarrow \lambda) L(z, \xi', \lambda') d\Omega(\xi') d\lambda'. \quad (4)$$

The Raman scattering phase function  $\beta_R$  can be obtained from the Raman absorption coefficient  $a_R$  and the Raman wavelength redistribution function  $f_R$  and expressed as

$$\left. \begin{aligned} \beta_R(\psi, \lambda' \rightarrow \lambda) &= b_R(\lambda' \rightarrow \lambda) \tilde{\beta}_R(\psi) \\ b_R(\lambda' \rightarrow \lambda) &= a_R(\lambda') f_R(\lambda' \rightarrow \lambda) \\ \beta_R(\lambda' \rightarrow \lambda, \psi) &= a_R(\lambda') f_R(\lambda' \rightarrow \lambda) \tilde{\beta}_R(\psi). \end{aligned} \right\} \quad (5)$$

The normalized phase function  $\tilde{\beta}_R(\psi)$  can be derived using scattering angle and the scattering angle can be found using Monte Carlo method

$$\tilde{\beta}^R(\psi) = 0.067(1 + 0.55 \cos^2 \psi). \quad (6)$$

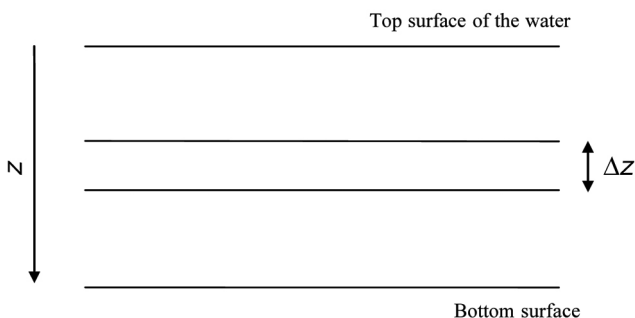


Figure 1. Representation of  $\Delta z$  at a particular depth  $z$ .

The value of  $\psi$  can be obtained using normalization condition from Monte Carlo methods. Let  $\gamma$  be the random number which can be derived from optical path length as follows

$$\gamma = 2\pi \int_0^\psi \tilde{\beta}(\psi') \sin \psi' d\psi', \quad (7)$$

where  $\gamma = 1 - \exp(-l)$ ,  $l$  is the optical path length and  $l = \zeta / |\mu|$ ,  $\zeta$  is the optical depth.

Mobley<sup>21</sup> derived the Raman wave number shift by the energy difference of the quantum state

$$\left. \begin{aligned} f^R(\lambda' \rightarrow \lambda) &= \frac{10^7}{\lambda^2} f^R \left[ 10^7 \left( \frac{1}{\lambda'} - \frac{1}{\lambda} \right) \right], \\ \text{where } f^R \left[ 10^7 \left( \frac{1}{\lambda'} - \frac{1}{\lambda} \right) \right] &= f^R(k''), \\ f^R(k'') &= \left[ \left( \frac{\pi}{4 \ln 2} \right)^{1/2} \sum_{i=1}^4 A_i \right]^{-1} \\ &\times \sum_{j=1}^4 A_j \frac{1}{k_j} \exp \left[ -4 \ln 2 \frac{(k'' - k_j)^2}{\Delta k_j^2} \right], \end{aligned} \right\} \quad (8)$$

where  $k''$  is the wave number shift of the Raman-scattered light relative to the wave number  $k'$  of the incident light,  $k_j$  is the centre of the  $j$ th Gaussian function,  $\Delta k_j$  the full width at half maximum of  $j$ th Gaussian function and  $A_j$  is the non-dimensional weight of the  $j$ th Gaussian function. Parameter values for the Raman wave number redistribution function  $f^R(k'')$  are taken from Mobley<sup>21</sup>.

The wavelength dependence of  $a_R$  can be expressed as

$$a_R(\lambda') = 2.6 \times 10^{-4} \times \left( \frac{488}{\lambda'} \right)^n. \quad (9)$$

From the investigations of Sugihara *et al.*<sup>24</sup>, the emitted wavelength ( $\lambda'$ ) is given by

$$\lambda' = \frac{\lambda}{1 - \Delta k \lambda}, \quad (10)$$

where  $\Delta k = 3.357 \times 10^{-4} \text{ nm}^{-1}$ .

Studies by Mobley<sup>21</sup>, and Pozdnyakov and Grass<sup>6</sup>, as well as other experimental studies found that the value of  $a_R$  is about  $2.6 \times 10^{-4} \text{ m}^{-1}$  at  $\lambda' = 488 \text{ nm}$  and  $n = 4$ .

Equation (4) can be simplified for the small wavelength interval  $\Delta \lambda'$ . The integration leads to

$$\begin{aligned} S_R(z, \xi, \lambda) &= \int_{4\pi} \beta_R(z, \xi' \rightarrow \xi, \lambda' \rightarrow \lambda) \\ &\times L(z, \xi', \lambda') d\Omega(\xi') \Delta \lambda'. \end{aligned} \quad (11)$$

From eq. (5) we get,

$$S_R(z, \theta, \phi, \lambda) = \Delta\lambda' a_R(\lambda') f_R(\lambda' \rightarrow \lambda) \times \int_0^{2\pi} \int_0^{\pi} \tilde{\beta}_R(\psi) L(z, \xi', \lambda') \sin \theta' d\theta' d\phi'. \quad (12)$$

For all the directions of  $\phi'$  the equation integrates to

$$S_R(z, \theta, \phi, \lambda) = 2\pi \times \Delta\lambda' a_R(\lambda') f_R(\lambda' \rightarrow \lambda) \times \int_0^{\pi} \tilde{\beta}_R(\psi) L(z, \xi', \lambda') \sin \theta' d\theta'. \quad (13)$$

For the given incident angle, the integration leads to the final Raman scattering source function as follows

$$S_R(z, \theta, \phi, \lambda) = 2\pi \times \Delta\lambda' a_R(\lambda') \times f_R(\lambda' \rightarrow \lambda) \tilde{\beta}_R(\psi) L(z, \xi', \lambda'). \quad (14)$$

### Fluorescence from phytoplankton

The fluorescence is quite different from the water Raman scattering function which is observed only in the presence of fluorescing material. Phytoplankton fluorescence is the isotropically emitted source due to the fluorescence of phytoplankton chlorophyll at 685 nm (ref. 15). Though the stimulating wavelength  $\lambda'$  varies, the emitting wavelength is nearly fixed around the red wavelength. Due to light absorption by phytoplankton, amplitude of the emission band depends on the excitation wavelength. Thus the source function for fluorescence from phytoplankton is expressed as

$$S_{Chl} = \int_0^{\lambda} \int_0^{4\pi} \beta_{F,Chl}(z, \xi' \rightarrow \xi, \lambda' \rightarrow \lambda) L(z, \xi', \lambda') d\Omega(\xi') d\lambda'. \quad (15)$$

According to Mobley<sup>21</sup>, the chlorophyll fluorescence phase function is defined as

$$\beta_{F,Chl}(\lambda' \rightarrow \lambda, \psi) = a_{F,Chl}(\lambda') f_{F,Chl}(\lambda' \rightarrow \lambda) \tilde{\beta}_{F,Chl}(\psi), \quad (16)$$

where  $a_{F,Chl}$  is the absorption due to chlorophyll fluorescence, which can be parameterized like the absorption coefficient of phytoplankton

$$a_{F,Chl} = a * c(\lambda') \times C_{Chl}(z), \quad (17)$$

with the specific absorption of chlorophyll  $a * c$  and concentration of chlorophyll  $C_{Chl}$ . Calculation of the wavelength redistribution function of fluorescence from

chlorophyll  $f_{F,Chl}$  requires knowledge of the fluorescence quantum yield of fluorescing components, ( $\eta_{F,Chl}$ ). Integrating  $\eta_{F,Chl}$  over all wavelengths gives the quantum efficiency of chlorophyll  $\Phi_{F,Chl}$  and it is found to be 0.0035 (ref. 5). The wavelength redistribution function  $f_{F,Chl}$  for the wavelengths from 370 to 690 nm can be rewritten as

$$f_{F,Chl}(\lambda' \rightarrow \lambda) = \Phi_{F,Chl} \times h_{Chl}(\lambda, \lambda_0, \sigma) \times \frac{\lambda'}{\lambda}. \quad (18)$$

Gokul *et al.*<sup>25</sup> presented a Gaussian function  $h_{Chl}$  which is expressed as

$$h_{Chl}(\lambda, \lambda_0, \sigma) = \frac{1}{\sqrt{2\pi}\sigma} \exp\left(-\frac{(\lambda - \lambda_0)^2}{2(\sigma)^2}\right), \quad (19)$$

where  $\lambda_0$  is the chlorophyll fluorescence peak at 685 nm with a full width and half maximum of 25 nm, yielding  $\sigma = 10.6$  nm.

The normalized phase function of  $\beta_{F,Chl}$  is given as

$$\tilde{\beta}_{F,Chl}(\psi) = \frac{1}{4\pi} \text{sr}^{-1}. \quad (20)$$

Equation (15) can be simplified for the small wavelength interval  $\Delta\lambda'$  and the integration leads to

$$S_{Chl}(z, \xi, \lambda) = \int_0^{4\pi} \beta_{F,Chl}(z, \xi' \rightarrow \xi, \lambda' \rightarrow \lambda) \times L(z, \xi', \lambda') d\Omega(\xi') \Delta\lambda'. \quad (21)$$

From eq. (16) we get

$$S_{Chl}(z, \theta, \phi, \lambda) = \Delta\lambda' a_{F,Chl}(\lambda') f_{F,Chl}(\lambda' \rightarrow \lambda) \times \int_0^{2\pi} \int_0^{\pi} \tilde{\beta}_{F,Chl}(\psi) L(z, \xi', \lambda') \sin \theta' d\theta' d\phi'. \quad (22)$$

For all the directions of  $\phi'$ , the equation integrates to

$$S_{Chl}(z, \theta, \phi, \lambda) = 2\pi \times \Delta\lambda' a_{F,Chl}(\lambda') f_{F,Chl}(\lambda' \rightarrow \lambda) \times \int_0^{\pi} \tilde{\beta}_{F,Chl}(\psi) L(z, \xi', \lambda') \sin \theta' d\theta'. \quad (23)$$

Substituting the value for  $\tilde{\beta}_{F,Chl}(\psi)$  we get

$$S_{Chl}(z, \theta, \phi, \lambda) = \frac{2\pi}{4\pi} \Delta\lambda' a_{F,Chl}(\lambda') f_{F,Chl}(\lambda' \rightarrow \lambda) \times \int_0^{\pi} L(z, \xi', \lambda') d\mu'. \quad (24)$$

For the given incident angle, integration leads to the final phytoplankton scattering source function as given below

$$S_{\text{Chl}}(z, \theta, \phi, \lambda) = 0.5 \times \Delta\lambda' a_{\text{F,Chl}}(\lambda') \times f_{\text{F,Chl}}(\lambda' \rightarrow \lambda) L(z, \xi', \lambda'). \quad (25)$$

*Fluorescence from coloured dissolved organics*

The position, shape and magnitude of the fluorescence peak of CDOM are slightly different from those of the chlorophyll for the varying incident wavelength, primarily due to the composition of CDOM substance which contains many kinds of humic and fulvic acids<sup>26</sup>. The source function for CDOM fluorescence is expressed as

$$S_{\text{CDOM}}(z, \xi, \lambda) = \int_0^\lambda \int_{0, 4\pi} \beta_{\text{F,CDOM}}(z, \xi' \rightarrow \xi, \lambda' \rightarrow \lambda) \times L(z, \xi', \lambda') d\Omega(\xi') d\lambda'. \quad (26)$$

The CDOM fluorescence phase function can be expressed similar to the chlorophyll fluorescence phase function

$$\beta_{\text{F,CDOM}}(\lambda' \rightarrow \lambda, \psi) = a_{\text{F,CDOM}}(\lambda') \times f_{\text{F,CDOM}}(\lambda' \rightarrow \lambda) \tilde{\beta}_{\text{F,CDOM}}(\psi), \quad (27)$$

where  $a_{\text{F,CDOM}}$  is the absorption due to CDOM fluorescence and expressed as

$$a_{\text{F,CDOM}} = a_{\text{CDOM}}(443) \times \exp(-S(\lambda - 443)). \quad (28)$$

Here  $S = 0.014$ . The wavelength redistribution function  $f_{\text{F,CDOM}}$  expressed using the spectral quantum efficiency function of CDOM fluorescence ( $\eta_{\text{F,CDOM}}$ ) is given as

$$f_{\text{F,CDOM}}(\lambda' \rightarrow \lambda) = \eta_{\text{F,CDOM}}(\lambda' \rightarrow \lambda) \times \frac{\lambda'}{\lambda}. \quad (29)$$

Using Hawes *et al.*<sup>26</sup>,  $\eta_{\text{F,CDOM}}$  is investigated by exhibiting wavelength shifts of the fluorescence and expressed as

$$\eta_{\text{F,CDOM}}(\lambda' \rightarrow \lambda) = A_0(\lambda') \exp \left\{ - \left[ \frac{\frac{1}{\lambda} - \frac{A_1}{\lambda'} - B_1}{0.6 \left( \frac{A_2}{\lambda'} + B_2 \right)} \right]^2 \right\}, \quad (30)$$

with  $A_1 = 0.470$ ,  $A_2 = 0.407$ ,  $B_1 = 8.077 \times 10^{-4} \text{ nm}^{-1}$  and  $B_2 = -4.57 \times 10^{-4} \text{ nm}^{-1}$ .

The normalized phase function due to CDOM fluorescence can be calculated similar to the chlorophyll as  $1/4\pi$ .

Equation (26) can be simplified for the small wavelength interval  $\Delta\lambda'$ . The integration leads to

$$S_{\text{CDOM}}(z, \xi, \lambda) = \int_{4\pi} \beta_{\text{F,CDOM}}(z, \xi' \rightarrow \xi, \lambda' \rightarrow \lambda) \times L(z, \xi', \lambda') d\Omega(\xi') \Delta\lambda'. \quad (31)$$

From eq. (27) we get

$$S_{\text{CDOM}}(z, \theta, \phi, \lambda) = \Delta\lambda' a_{\text{F,CDOM}}(\lambda') f_{\text{F,CDOM}}(\lambda' \rightarrow \lambda) \times \int_0^{2\pi} \int_0^\pi \tilde{\beta}_{\text{F,CDOM}}(\psi) L(z, \xi', \lambda') \sin \theta' d\theta' d\phi'. \quad (32)$$

For all the directions of  $\phi'$ , the equation integrates to

$$S_{\text{CDOM}}(z, \theta, \phi, \lambda) = 2\pi \times \Delta\lambda' a_{\text{F,CDOM}}(\lambda') f_{\text{F,CDOM}}(\lambda' \rightarrow \lambda) \times \int_0^\pi \tilde{\beta}_{\text{F,CDOM}}(\psi) L(z, \xi', \lambda') \sin \theta' d\theta'. \quad (33)$$

The normalized phase function  $\tilde{\beta}_{\text{F,CDOM}}(\psi)$  is defined as

$$\tilde{\beta}_{\text{F,CDOM}}(\psi) = \frac{1}{4\pi} \text{sr}^{-1}. \quad (34)$$

Substituting this in eq. (33) leads to

$$S_{\text{CDOM}}(z, \theta, \phi, \lambda) = \frac{2\pi}{4\pi} \Delta\lambda' a_{\text{F,CDOM}}(\lambda') \times f_{\text{F,CDOM}}(\lambda' \rightarrow \lambda) \int_0^\pi L(z, \xi', \lambda') d\mu'. \quad (35)$$

For the given incident angle, the integration leads to the final CDOM scattering source function as

$$S_{\text{CDOM}}(z, \theta, \phi, \lambda) = 0.5 \Delta\lambda' a_{\text{F,CDOM}}(\lambda') \times f_{\text{F,CDOM}}(\lambda' \rightarrow \lambda) L(z, \xi', \lambda'). \quad (36)$$

*Radiative transfer model*

Inclusion of these source functions in the basic RTE leads to

$$\begin{aligned} \mu \frac{dL(z, \xi, \lambda)}{dz} &= -c(z, \lambda)L(z, \xi, \lambda) \\ &+ \int_{\Xi} L(z, \xi', \lambda) \beta(z, \xi' \rightarrow \xi, \lambda) d\Omega(\xi') + S_{\text{Chl}}(z, \xi, \lambda) \\ &+ S_{\text{R}}(z, \xi, \lambda) + S_{\text{CDOM}}(z, \xi, \lambda). \end{aligned} \quad (37)$$

On integration we get

$$\begin{aligned} \mu \frac{dL(z, \xi, \lambda)}{dz} &= -c(z, \lambda)L(z, \xi, \lambda) \\ &+ \frac{b(z, \lambda)}{4\pi} \int_{\Xi} L(z, \xi', \lambda) d\Omega(\xi') + S_{\text{Chl}}(z, \xi, \lambda) \\ &+ S_{\text{R}}(z, \xi, \lambda) + S_{\text{CDOM}}(z, \xi, \lambda). \end{aligned} \quad (38)$$

Considering a given incident angle, the integration leads to the following expression

$$\begin{aligned} \mu \frac{dL(z, \xi, \lambda)}{dz} &= -c(z, \lambda)L(z, \xi, \lambda) \\ &+ \frac{b(z, \lambda)}{2} L(z, \xi', \lambda) + S_{\text{Chl}}(z, \xi, \lambda) \\ &+ S_{\text{R}}(z, \xi, \lambda) + S_{\text{CDOM}}(z, \xi, \lambda). \end{aligned} \quad (39)$$

Solving this differential equation with the assumption for the particular depth interval  $\Delta z$  leads to

$$\begin{aligned} L(z, \xi, \lambda) &= c \times \exp \\ &\times \left[ \begin{aligned} &\left( -c(z, \lambda) + \frac{b(z, \lambda)}{2} + \right. \\ &(0.5 \times \Delta \lambda' a_{\text{F,Chl}}(\lambda') f_{\text{F,Chl}}(\lambda' \rightarrow \lambda)) + \\ &(2\pi \times \Delta \lambda' a_{\text{R}}(\lambda') f_{\text{R}}(\lambda' \rightarrow \lambda) \tilde{\beta}_{\text{R}}(\psi)) + \\ &\left. \frac{(0.5 \Delta \lambda' a(\lambda') f_{\text{F,CDOM}}(\lambda' \rightarrow \lambda)) f_{\text{F,CDOM}}}{\mu} \right) \times \Delta z \end{aligned} \right]. \end{aligned} \quad (40)$$

According to Beer's law, the above equation can be written as

$$\begin{aligned} L(z, \xi, \lambda) &= L(0, \xi, \lambda) \times \exp \\ &\times \left[ \begin{aligned} &\left( -c(z, \lambda) + \frac{b(z, \lambda)}{2} + \right. \\ &(0.5 \times \Delta \lambda' a_{\text{F,Chl}}(\lambda') f_{\text{F,Chl}}(\lambda' \rightarrow \lambda)) + \\ &(2\pi \times \Delta \lambda' a_{\text{R}}(\lambda') f_{\text{R}}(\lambda' \rightarrow \lambda) \tilde{\beta}_{\text{R}}(\psi)) + \\ &\left. \frac{(0.5 \times \Delta \lambda' a(\lambda') f_{\text{F,CDOM}}(\lambda' \rightarrow \lambda)) f_{\text{F,CDOM}}}{\mu} \right) \times \Delta z \end{aligned} \right]. \end{aligned} \quad (41)$$

## Results and discussion

Inputting the measured IOP data into the present model and Hydrolight model, we simulated upwelling radiances with the effects of inelastic scattering in relatively clear water (low sediments, CDOM and chlorophyll), turbid water (high sediments, low CDOM and chlorophyll), and productive water (high chlorophyll and CDOM). The results of our model were compared with depth-dependant measured upwelling radiance data and the results from the Hydrolight numerical model (Figure 2). Our simulation results indicate that when incorporating the effect of Raman scattering on spectral variations of the upwelling radiance, arising from relatively clear waters (chlorophyll = 0.2–0.5 mg m<sup>-3</sup>; suspended sediments 0.09–0.8 g m<sup>-3</sup>;  $a_{\text{CDOM}}(443) = 0.01 \text{ m}^{-1}$ ),  $L_u(\lambda)$  increases with wavelength reaching a maximum around 450–490 nm, which is then followed by a steep fall-off at longer wavelengths. In turbid waters (chlorophyll 1.0–1.5 mg m<sup>-3</sup>; suspended sediments 12.3–50.2 g m<sup>-3</sup>;  $a_{\text{CDOM}}(443) = 0.03 \text{ m}^{-1}$ ),  $L_u(\lambda)$  increases with wavelength reaching a maximum at green and red wavelengths. These variations in the resultant upwelling radiance comply with those reported by Waters<sup>27</sup>, and Grassl *et al.*<sup>7</sup>. A similar behaviour is observed in phytoplankton-dominated productive waters (chlorophyll 101–345 mg m<sup>-3</sup>; suspended sediments 42–120 g m<sup>-3</sup>;  $a_{\text{CDOM}}(443) = 5.04\text{--}8.03 \text{ m}^{-1}$ ), but there is an increase in  $L_u(\lambda)$  values at wavelengths >685 nm, although such effect is substantially reduced across the visible wavelengths as this water body contains admixtures of the three colourants.

On the contrary, fluorescence from chlorophyll manifests as a Gaussian distribution centred on the peak chlorophyll fluorescence emission wavelength around 685 nm (ref. 28). Thus, this spectral distribution is expected to be a prominent feature of upwelling radiance from waters rich in chlorophyll, and this feature would further increase in prominence and shift towards the longer wavelengths as the concentration of chlorophyll increases in more productive and eutrophic waters<sup>22,29</sup>. In turbid and productive waters, the effects of CDOM and chlorophyll fluorescence on  $L_u(\lambda)$  are similar at  $\lambda < 600 \text{ nm}$ , but become well pronounced at higher wavelengths. In particular, the spectral region within which the resultant upwelling radiance is affected by fluorescence is >680 nm for chlorophyll and 450–600 nm for dissolved organics in bloom-dominated productive waters. These results are in compliance with other studies and measurements<sup>7,30,31</sup>. The contribution of the dissolved organics is also noticeably high at wavelengths around 685–730 nm, likely due to high dissolved substances associated with phytoplankton production in such waters. This study seems to provide evidence of the actual manifestation of dissolved organics fluorescence in highly eutrophic lagoon (productive) waters. Our results also show that fluorescence mechanisms influence the colour of coastal and inland

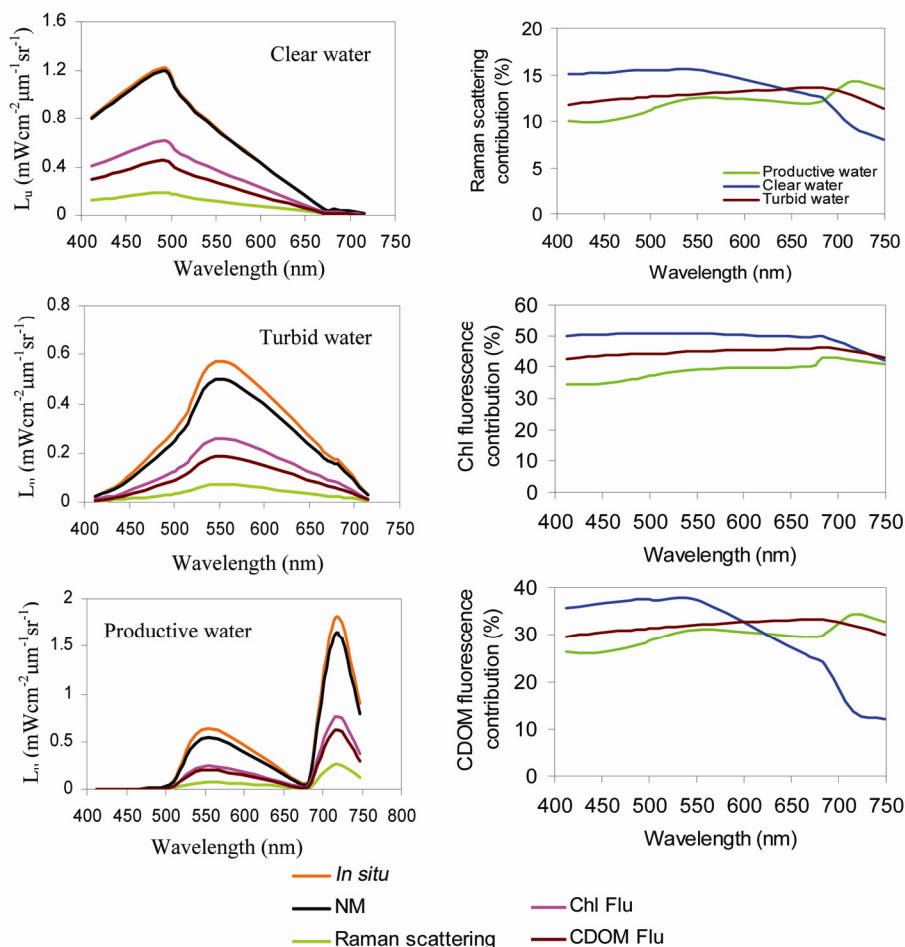


**Figure 2.** Left panels: Effects of water Raman scattering, chlorophyll fluorescence and CDOM fluorescence on the upwelling radiances from clear water, turbid water (sediment-laden) and productive water (phytoplankton and CDOM dominated). Right panels: The percentage contributions of Raman scattering, chlorophyll fluorescence and CDOM fluorescence on the upwelling radiances from these three waters. Note that the simulated upwelling radiances (new model-NM) are better consistent with measured data.

water bodies, especially when the concentration of the fluorophores is relatively higher than that of mineral sediments in such waters. In turbid coastal waters, increasing concentration of suspended sediments rapidly and effectively dampens the impacts of chlorophyll and CDOM fluorescence on the upwelling spectra, as also evident from their percentage contribution spectra which appear to be nearly spectrally flat, especially at green and red wavelengths. Therefore, a fluorescence signal in the spectral distribution of upwelling radiance can be easily detected in waters rich in phytoplankton and dissolved organics, but not in strongly scattering waters.

These results indicate that the impact of trans-spectral processes on upwelling radiance is controlled essentially by in-water optical conditions. In the previous studies, water Raman scattering was reported to be of limited importance in clear waters nearly devoid of other optically substances. However, the present study demonstrates that its effect cannot be ignored in such waters. It also shows evidence of the fluorescence of chlorophyll and dissolved

organics to be capable of influencing upwelling radiance and eventually the retrieval of concentrations of water constituents with bio-optical algorithms derived without due reference to trans-spectral effects in coastal and inland water types<sup>7</sup>. In such cases, the error of the atmospheric correction should be substantially lower than that induced by the trans-spectral effects<sup>2,3</sup>.

The upwelling radiances generated with the effects of water Raman scattering, CDOM and phytoplankton fluorescence from the present model and Hydrolight model for clear, turbid and productive waters, are compared with measured upwelling radiances from three discrete depths (Figures 3–5). In clear waters, IOPs are constant for a more depth interval ( $\Delta z$ ) at a particular depth  $z$  and these  $\Delta z$  values depend on the turbidity of the water. In this case,  $\Delta z$  values are  $\sim 3$  m, as the variation of turbidity is minimal. Also, IOPs are assumed to be constant for a particular wavelength interval ( $\Delta \lambda$ ) (here the wavelength interval is taken as 1 nm, i.e.  $\Delta \lambda = 1$  nm). Comparison shows that simulated upwelling radiances from the new

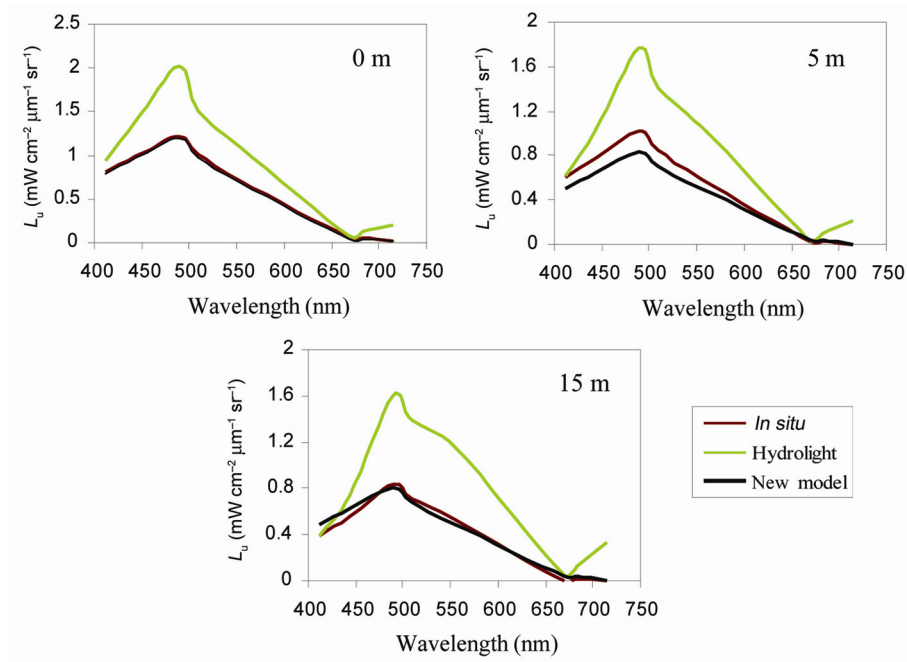


**Figure 3.** Comparison of the simulated upwelling radiances ( $L_u(\lambda)$ ) from the new model and Hydrolight model with measured upwelling radiance data from three discrete depths in clear water off Chennai.

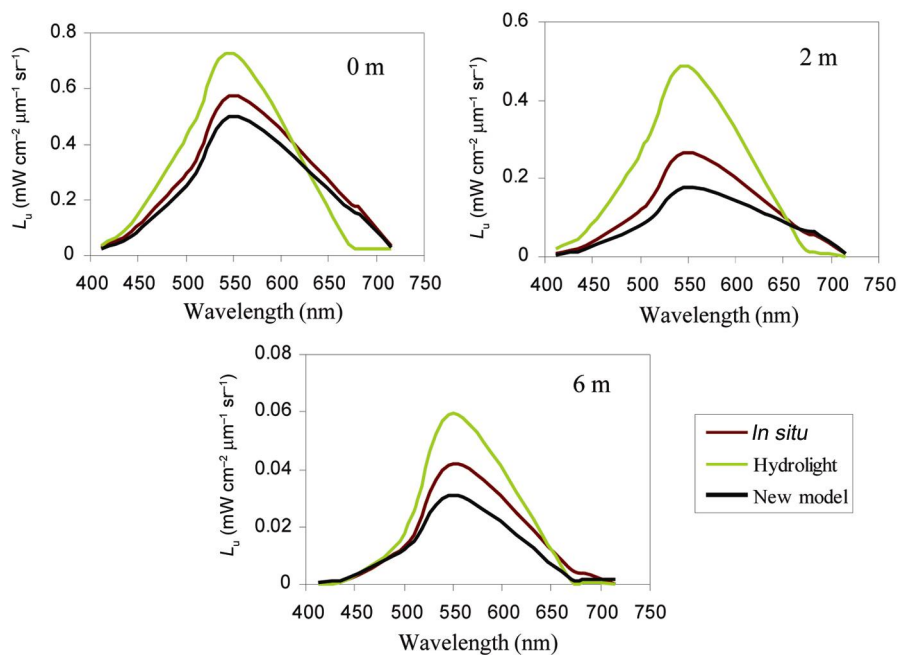


**Figure 4.** Comparison of the simulated upwelling radiances ( $L_u(\lambda)$ ) from the new model and Hydrolight model with measured upwelling radiance data from three discrete depths in turbid coastal water off Point Calimere.

model are in good agreement with measured data (Figure 3). By contrast, the Hydrolight model tends to overestimate the measured spectral upwelling radiance in the blue–red wavelength region. In turbid waters (sediment-dominated), IOPs are constant for a small depth interval ( $\Delta z$ ) at a particular depth  $z$  compared to those measured from clear waters, and  $\Delta z$  values in this case range from

2.5 cm to 50 cm because of the fluctuation of turbidity along the depth. Further, IOPs are assumed to be constant for a particular wavelength interval ( $\Delta\lambda$ ) ( $= 1$  nm). Figure 4 compares the simulated upwelling radiance with the measured data in turbid coastal waters. It becomes obvious that the Hydrolight model predicts upwelling radiances much higher than the measured data, whereas the

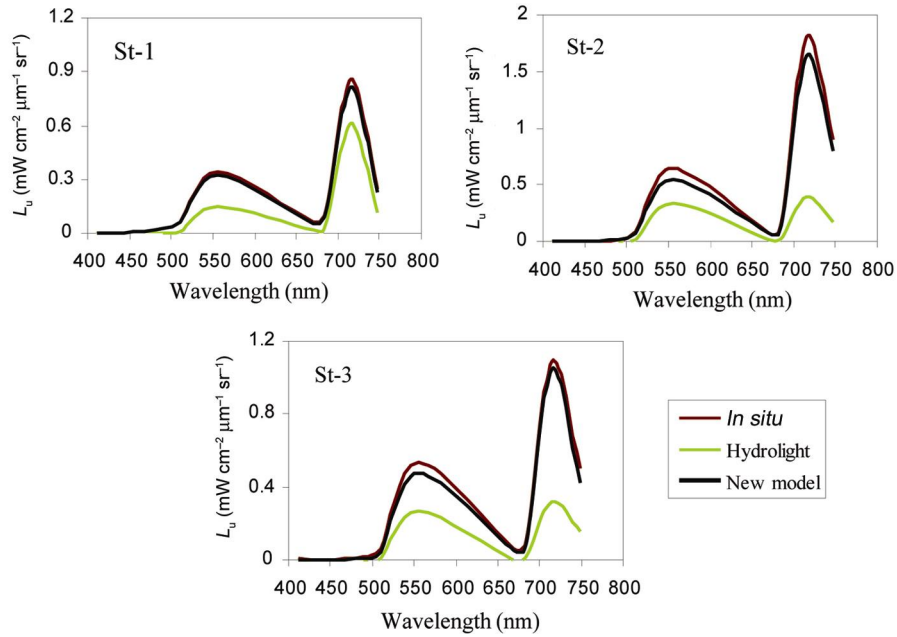


**Figure 5.** Comparison of the simulated upwelling radiances ( $L_u(\lambda)$ ) from the new model and Hydrolight model with measured upwelling radiance data from three different stations in productive waters (lagoon water) around Chennai.

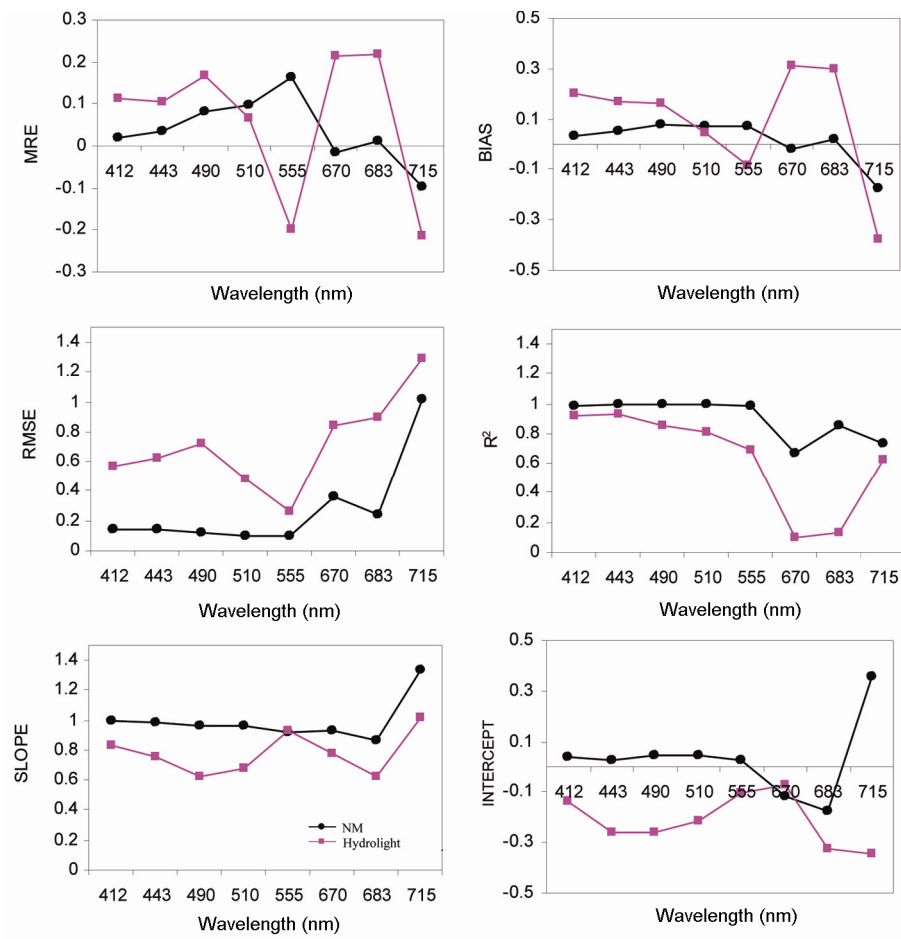


**Figure 6.** Results of the statistical analyses performed between the simulated and measured upwelling radiance data from all three waters. RMSE, Root mean square error; MRE, Mean relative error, and  $R^2$ , Determination coefficient. These error plots are made only for a few wavelengths for brevity. NM, New model.

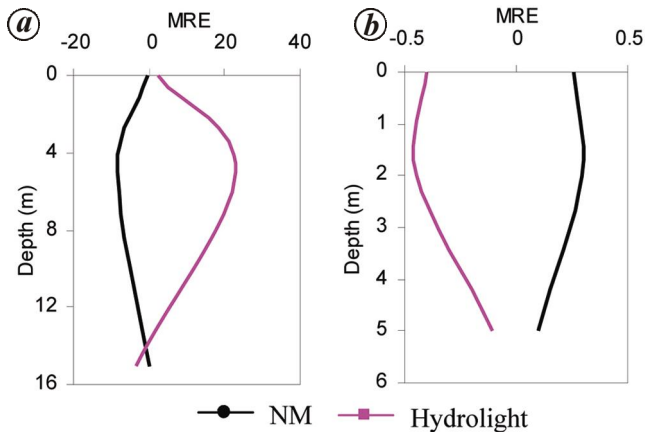


**Figure 7.** Mean relative error (MRE) along the depth at two different stations from clear water (a) and turbid water (b) for the new model (NM) and Hydrolight numerical model.

present model yields  $L_u(\lambda)$  more closer to the *in situ* data for all the three depths. Similar results are observed in productive waters (Figure 5), where the depth is around 3–5 feet and hence surface measurement data were only possible. The new model is effective in terms of yielding more accurate  $L_u(\lambda)$  spectra capturing the effects of Raman scattering, CDOM and phytoplankton fluorescence. In this case, the Hydrolight model tends to underestimate the upwelling radiances across the entire visible wavelengths (Figure 5).

Statistical analyses performed on these *in situ* and simulated  $L_u(\lambda)$  data further indicate low errors (mean relative error, root means square error, bias and intercept), and high slope and  $R^2$  values for the new model (Figure 6). Errors associated with the Hydrolight model are significantly higher because of its  $L_u(\lambda)$  values drifting from the measured  $L_u(\lambda)$  values in clear, turbid and productive waters. Figure 7 shows the depth-wise variation of error for moderately turbid and clear waters. Again, the Hydrolight model tends to yield high errors along the depth. The present model is more accurate and thus yields low errors regardless of the variations of the optically active constituents in the water column.

## Conclusion

The results of this study suggest that the impact of trans-spectral processes on upwelling radiance from clear, turbid and productive waters is significant. In particular, the effect of CDOM and chlorophyll fluorescence on upwelling radiance is most significant in productive coastal and inland waters, wherein chlorophyll pigment is the overwhelmingly dominant optically active constituent. The impact of chlorophyll fluorescence on upwelling radiance cannot be neglected in case 1 waters that are considered to be solely dominated by phytoplankton. In turbid coastal waters, suspended sediments reduce the

effects of chlorophyll and CDOM fluorescence on upwelling radiance. On the other hand, the relative contribution of water Raman scattering to upwelling radiance is higher in clear oceanic waters and lower in turbid and productive coastal/inland waters. This implies that neglecting the impacts of trans-spectral effects in inverse models can introduce errors in the derived products from hyperspectral satellite data for many inland and coastal water bodies. In such cases of waters rich in optically active substances, previous studies<sup>7,22</sup> have suggested to make use of the field-determined optical cross-section spectra and multivariate optimization techniques to mitigate the impacts of trans-spectral processes in remotely estimating co-existing concentrations of water constituents in coastal and inland water bodies. However, such approaches would become reasonable only if the error of the atmospheric correction is substantially lower than the one introduced by the trans-spectral effects. Though atmospheric correction is a difficult problem, accurate water-leaving radiance products over such optically complex water bodies are now possible with an approach proposed by Shanmugam<sup>2</sup>, and Rakesh Kumar and Shanmugam<sup>3</sup>. Therefore, with the modern computational facilities and improved atmospheric correction and retrieval algorithms for satellite data, more accurate water quality parameters can be derived for various applications in coastal and inland waters.

1. Pravin, P. J. and Shanmugam, P., A new theory and its application to remove the effect of surface-reflected light in above-surface radiance data from clear and turbid waters. *J. Quant. Spectrosc. Radiat. Transf.*, 2014, **142**, 75–92.
2. Shanmugam, P., CAAS: an atmospheric correction algorithm for the remote sensing of complex waters. *Ann. Geophys.*, 2012, **30**, 203–220.
3. Rakesh Kumar, S. and Shanmugam, P., A novel method for estimation of aerosol radiance and its extrapolation in the atmospheric correction of satellite data over optically complex oceanic waters. *Remote Sensing Environ.*, 2014, **142**, 188–206.
4. Sundarabalan, B., Shanmugam, P. and Manjusha, S., Radiative transfer modelling of upwelling light field in coastal waters. *J. Quant. Spectrosc. Radiat. Transf.*, 2013, **121**, 30–44.
5. Schroeder, M., Barth, H. and Reuter, R., Effect of inelastic scattering on underwater daylight in the ocean: model evaluation, validation, and first results. *Appl. Opt.*, 2003, **42**, 4244–4260.
6. Pozdnyakov, D. V. and Grassl, H., *Colour of Inland and Coastal Waters: Methodology for its Interpretation*, Springer-Praxis, Chichester, 2003, p. 170.
7. Grassl, H., Pozdnyakov, D., Lyaskovsky, A. and Pettersson, L., Numerical modelling of transspectral processes in natural waters: implications for remote sensing. *Int. J. Remote Sensing*, 2010, **23**, 1581–1607.
8. Westberry, T. K., Boss, E. and Lee, Z., Influence of Raman scattering on ocean colour inversion models. *Appl. Opt.*, 2013, **52**, 5552–5561.
9. Gordon, H. R., Lewis, M. R., McLean, S. D., Twardowski, M. S., Freeman, S. A., Voss, K. J. and Boynton, G. C., Spectra of particulate backscattering in natural waters. *Opt. Exp.*, 2009, **17**, 16192–16208.
10. Lee, Z. P., Carder, K. L., Hawes, S. K., Steward, R. G., Peacock, T. G. and Davis, C. O., Model for the interpretation of hyperspectral remote-sensing reflectance. *Appl. Opt.*, 1994, **33**, 5721–5732.

11. Sathyendranath, S. and Platt, T., Ocean-colour model incorporating transpectral processes. *Appl. Opt.*, 1998, **37**, 2216–2227.
12. Fukuzaki, K., Imai, I., Fukushima, K., Ishii, K.-I., Sawayama, S. and Yoshioka, T., Fluorescent characteristics of dissolved organic matter produced by bloom-forming coastal phytoplankton. *J. Plankton Res.*, 2014, **36**(3), 685–694.
13. Dekker, A. G., Detection of optical water quality parameters for eutrophic waters by high resolution remote sensing. Vrije Universiteit, Amsterdam, 1993, pp. 1–240.
14. Gitelson, A., The peak near 700 nm on radiance spectra of algae and water: relationships of its magnitude and position with chlorophyll concentration. *Int. J. Remote Sensing*, 1992, **13**(17), 3367–3373.
15. Gordon, H. R., Diffuse reflectance of the ocean: the theory of its augmentation by chlorophyll-fluorescence at 685 nm. *Appl. Opt.*, 1979, **18**(8), 1161–1167.
16. Kishino, M., Sugihara, S. and Okami, N., Theoretical analysis of the *in situ* fluorescence of chlorophyll *a* on the underwater spectral irradiance. *Bulletin de la Societe Franco-Japonaise d'Océanographie*, 1986, **24**, 130–138.
17. Babin, M., Morel, A. and Gentili, B., Remote sensing of sea surface sun-induced chlorophyll fluorescence – consequences of natural variations in the optical characteristics of phytoplankton and the quantum yield of chlorophyll *a* fluorescence. *Int. J. Remote Sensing*, 1996, **17**, 2417–2448.
18. Brando, V. E. and Dekker, A. G., The fluorescence term on the observed 690–710 nm reflectance peak in eutrophic turbid (inland) waters: myth or reality? *Ocean Optics*, 2002, **XVI**, 1–13.
19. Pope, R. M. and Fry, E. S., Absorption spectrum (380–700 nm) of pure water. II. Integrating cavity measurements. *Appl Opt.*, 1997, **36**, 8710–8723.
20. Smith, R. C. and Baker, K. S., Optical properties of the clearest natural waters (200–800 nm). *Appl. Opt.*, 1981, **20**, 177–184.
21. Mobley, C. D., *Light and Water: Radiative Transfer in Natural Waters*, Academic Press, San Diego, 1994, pp. 472–476.
22. Bukata, R. P., Jerome, J. H., Borstad, G. A., Brown, L. N. and Gower, J. F. R., Mitigating the impact of trans-spectral processes on multivariate retrieval of water quality parameters from case 2 waters. *Can. J. Remote Sensing*, 2004, **30**, 8–16.
23. Raman, C. V. and Krishnan, K. S., A new type of secondary radiation. *Nature*, 1928, **121**, 501–502.
24. Sugihara, S., Kishino, M. and Okami, N., Contribution of Raman scattering to upward irradiance in the sea. *J. Oceanogr. Soc. Jpn*, 1984, **40**, 397–404.
25. Gokul, E. A., Shanmugam, P., Sundarabalan, B., Sahay, A. and Chauhan, P., Modelling the inherent optical properties and estimating the constituents 'concentrations in turbid and eutrophic waters. *Cont. Shelf Res.*, 2014, **84**, 120–138.
26. Hawes, S. K., Carder, K. L. and Harvey, G. R., Quantum fluorescence efficiencies of fulvic and humic acids: effects on ocean colour and fluorometric detection. In *Ocean Optics XI*, Proceedings of the Society of Photo-Optical Instrumentation Engineers, Bellingham, WA, Int. Soc. Opt. Eng., 1992, pp. 212–223.
27. Waters, K. J., Effects of Raman scattering on water-leaving radiance. *J. Geophys. Res.*, 1995, **100**, 13151–13161.
28. Ahn, Y. H. and Shanmugam, P., Derivation and analysis of the fluorescence algorithms to estimate chlorophyll *a* concentrations in ocean waters. *J. Opt. A: Pure Appl. Opt.*, 2007, **9**, 352–362.
29. Gitelson, A. A., Yacobi, Y. Z., Schalles, J. F., Rundquist, D. C., Han, L., Stark, R. and Etzion, D., Remote estimation of phytoplankton density in productive waters. *Adv. Limnol.*, 2000, **55**, 121–136.
30. Culver, M. E. and Perry, M. J., Calculation of solar-induced fluorescence in surface and subsurface waters. *J. Geophys. Res.*, 1997, **102**, 563–572.
31. Vodacek, A., Green, S. A. and Blough, N. V., An experimental model of the solar-stimulated fluorescence of chromophoric dissolved organic matter. *Limnol. Oceanogr.*, 1994, **39**, 1–11.

ACKNOWLEDGEMENTS. This work was supported by the Indian Institute of Technology (IIT) Madras through the fellowship awarded to J. Vigneshwaran. We thank D. Rajshekhar, Head, Vessel Management Cell and Director, National Institute of Ocean Technology, for providing the coastal research vessels *Sagar Manjusha* and *Sagar Paschimi* to IIT Madras for carrying out various above-water and underwater measurements in coastal waters off Point Calimere and Chennai.